Vol. 10, No. 01 (2026) 15 – 27
JIIF (Jurnal Ilmu dan Inovasi Fisika)
https://jurnal.unpad.ac.id/jiif/
UNPAD
SINTA 3

INVERSION METHOD FOR CALCULATING ILL CONDITIONING IN DYNAMIC LIGHT SCATTERING (DLS) SYSTEM: APPLICATION TO POLYDISPERSE SILICA SUSPENSION

EGIS RISZEKIYA[1], SETIANTO[2], LIU KIN MEN[2], FERRY FAIZAL[2,*]

[1]*Physics Study Program, Universitas Padjadjaran*
[2]*Department of Physics, Universitas Padjadjaran*
Jl. Raya Bandung-Sumedang Km.21 Jatinangor 45363, Sumedang, Jawa Barat, Telp. 022-7796014

**Corresponding author*
Email: ferry.faizal@unpad.ac.id

Submitted: 24/11/2025
Accepted: 26/01/2026
Published: 12/02/2026

Abstract. This study presents the development and evaluation of a self-constructed Dynamic Light Scattering system using a digital oscilloscope as its main acquisition platform. The aim of this research is to investigate the ability of the oscilloscope-based approach to measure particle size distributions and to compare its performance with that of a conventional Dynamic Light Scattering instrument. Autocorrelation data collected at different temporal acquisition settings were processed using Tikhonov regularization, and the optimal regularization parameter was determined through analysis of the characteristic L-shaped curve. The results show that the temporal resolution of the oscilloscope strongly influences the stability and accuracy of the reconstructed particle size distributions. Measurements obtained at medium acquisition intervals provide the best agreement with the commercial system, producing sharp and well-defined particle size peaks. In contrast, excessively short or long acquisition windows introduce noise or loss of temporal detail, which affects the inversion results. Overall, the findings demonstrate that an oscilloscope-based Dynamic Light Scattering approach can serve as an effective and low-cost alternative for particle size characterization and has strong potential for future development into a portable and affordable optical measurement system.

Keywords: Dynamic light scattering, nanoparticle, particle size distribution, oscilloscope measurement, Tikhonov regularization

Abstrak. *Penelitian ini menyajikan pengembangan dan evaluasi sistem Dynamic Light Scattering swakriya yang menggunakan osiloskop digital sebagai platform akuisisi utama. Tujuan penelitian ini adalah untuk mengkaji kemampuan pendekatan berbasis osiloskop dalam mengukur distribusi ukuran partikel serta membandingkan kinerjanya dengan instrumen Dynamic Light Scattering konvensional. Data autokorelasi yang dikumpulkan pada berbagai pengaturan waktu akuisisi diproses menggunakan regularisasi Tikhonov, dan nilai parameter optimum ditentukan melalui analisis kurva berbentuk huruf L yang khas. Hasil penelitian menunjukkan bahwa resolusi temporal dari osiloskop sangat mempengaruhi stabilitas dan akurasi rekonstruksi distribusi ukuran partikel. Pengukuran yang diperoleh pada interval akuisisi menengah memberikan kesesuaian terbaik dengan sistem komersial, menghasilkan puncak distribusi ukuran yang tajam dan terdefinisi dengan baik. Sebaliknya, jendela akuisisi*

DOI: https://doi.org/10.24198/jiif.v10i1.68294 *e-ISSN: 2549-7014*

yang terlalu pendek atau terlalu panjang menyebabkan munculnya derau atau hilangnya detail temporal yang mempengaruhi hasil inversi. Secara keseluruhan, temuan ini menunjukkan bahwa pendekatan Dynamic Light Scattering berbasis osiloskop dapat menjadi alternatif yang efektif dan berbiaya rendah untuk karakterisasi ukuran partikel, serta memiliki potensi besar untuk dikembangkan menjadi sistem optik portabel dan terjangkau di masa mendatang.

Kata kunci: *Dynamic Light Scattering, nanopartikel, distribusi ukuran partikel, pengukuran osiloskop, regularisasi Tikhonov*

1. Introduction

Nanoparticles have become increasingly pivotal in modern science and engineering, being used in applications from catalysis and biomedical imaging to photonic devices and environmental sensing. The properties of these nanoparticles are strongly influenced by their size distribution, which governs parameters such as surface to volume ratio (SAVR), Brownian diffusion behavior, and light scattering cross sections in colloidal suspensions [1]. Similarly, accurate determination of particle size distribution (PSD) is critical in nanomaterials research, as observed in comparative studies of various inversion techniques [2]. For example is silica material which processed from nature have board distribution (polydisperse), so PSD determine need a looping for in different order (nanometer, sub-micrometer, and micrometer) [3]. Among the available characterization techniques, Dynamic Light Scattering (DLS) stands out for its non invasive nature, rapid measurement, and statistical averaging over many particles. DLS tracks the temporal fluctuations in scattered light intensity due to Brownian motion of particles, converts these fluctuations into an autocorrelation function, and maps that into diffusion coefficients and hydrodynamic diameters via the Stokes Einstein relation [4]. Yet the practical limitations of DLS such as sensitivity to particle concentration, polydispersity, and number fluctuations have been highlighted in recent reviews of DLS under ultra-low concentrations [5].

However, the mathematical mapping from the measured autocorrelation function to PSD is fundamentally an ill-posed inverse problem, the kernel linking correlation decay rates to size distribution corresponds to a Fredholm integral equation of the first kind, which is ill conditioned and prone to noise amplification [6]. Conventional algorithmic approaches, such as cumulant analysis or unconstrained inversion, can yield unstable or non physical distributions, especially for multimodal or highly polydisperse samples [7]. To mitigate the instability of PSD reconstruction in DLS, regularisation techniques such as the Tikhonov regularization method are widely used, this approach adds a penalty term on the solution norm (or its derivatives) to stabilise the inversion and improve robustness [8]. The selection of the regularisation parameter (α) is critical and methods such as the L-curve have been proposed and applied in DLS contexts [9].

Despite algorithmic advances, two major challenges remain in DLS instrumentation and data processing. First, commercial DLS systems incorporate proprietary hardware and software that limit transparency and customization, and their high cost can restrict access for many research labs [10]. Second, while some low cost or custom DLS setups are reported in literature, many of them lack a rigorous inversion algorithm to reliably convert the raw correlation data into PSD leading to qualitative rather than quantitative results [11].

In this work, we present an affordable DLS system that combines a digital oscilloscope (GDS-2104) for real-time signal acquisition with a photodiode (OPT101) for detecting scattered light intensity. The system is used to measure a silica (SiO_2) suspension prepared by previous method explained elsewhere [12], and the collected correlation data are processed via a Python-based inversion framework using Tikhonov regularization. Our aims are to validate this affordable DLS setup against a commercial DLS analyser and to implement a transparent inversion algorithm for the ill-conditioned DLS kernel.

2. Research Methods

2.1 Data Acquisition

The DLS measurement system is designed to characterize nanoparticle sizes using a homodyne scattering configuration with a laser wavelength of 650 nm. The light source is directed toward a measurement chamber containing the SiO_2 sample placed in a glass cuvette, while the detector is positioned perpendicular to the incident beam to capture the scattered light intensity. The analog signal from the light detector (OPT101 photodiode, spectral response 400–1000 nm) is digitized using a GDS-2104 digital oscilloscope with a sampling rate of up to 1 GS/s and an 8-bit vertical resolution [13, 14]. The acquired data are stored as a time series I(t), representing the scattered light intensity as a function of time. The entire system is controlled via a serial/USB interface using a Python script for automated data acquisition and storage.

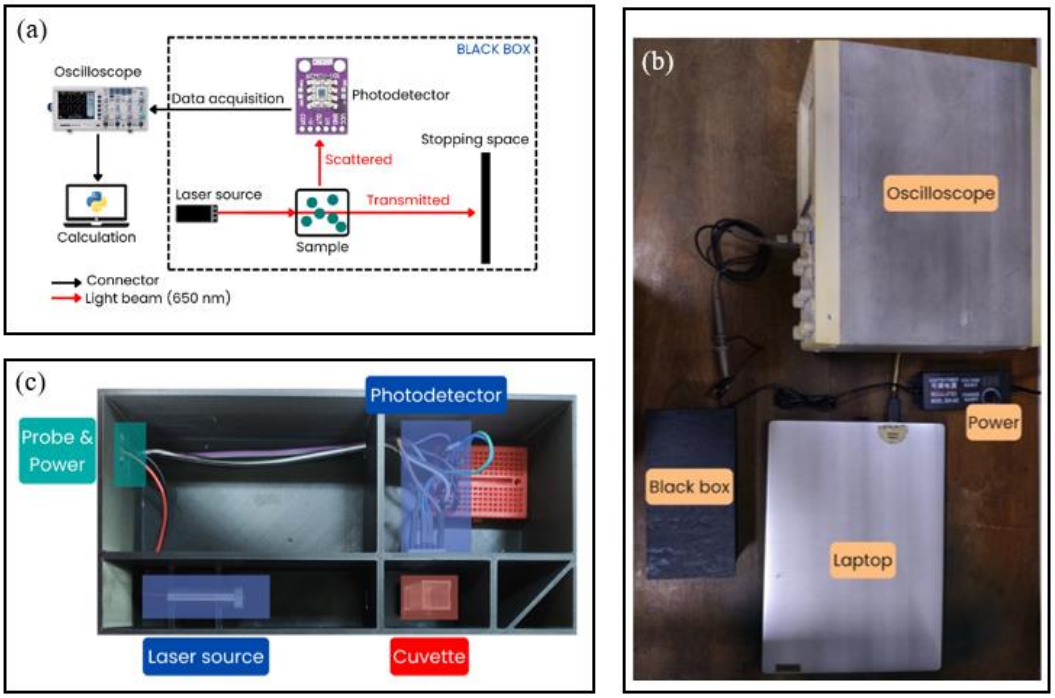

Figure 1. (a) Schematic diagram of the self-constructed DLS system. A 650 nm laser source illuminates the nanoparticle sample inside a glass cuvette, producing both transmitted and scattered light. The scattered light is collected by a photodetector and transferred to the oscilloscope for data acquisition, while subsequent calculations are performed on a computer. All optical components are placed inside a black enclosure to minimize ambient light interference; (b) Experimental setup in the laboratorium showing the oscilloscope, the black enclosure containing the optical components, the power supply, and the laptop used for data processing; (c) Internal arrangement of the black enclosure, illustrating the positioning of the laser source, cuvette, photodetector, and probe connections.

The workflow shown in the diagram (figure 2) illustrates the complete measurement and inversion process used to obtain PSD from DLS data acquired with a digital oscilloscope. First, a coherent laser beam is directed at a suspension of nanoparticles, where the random Brownian motion of the particles induces temporal fluctuations in the intensity of the scattered light. This scattered light is collected at a fixed angle 90° using a photodiode detector (OPT101), which converts the optical intensity fluctuations into an analog electrical signal. The resulting time-varying voltage is then recorded in real time by a digital oscilloscope (GDS-2104), producing a discrete intensity time series that reflects the underlying particle dynamics.

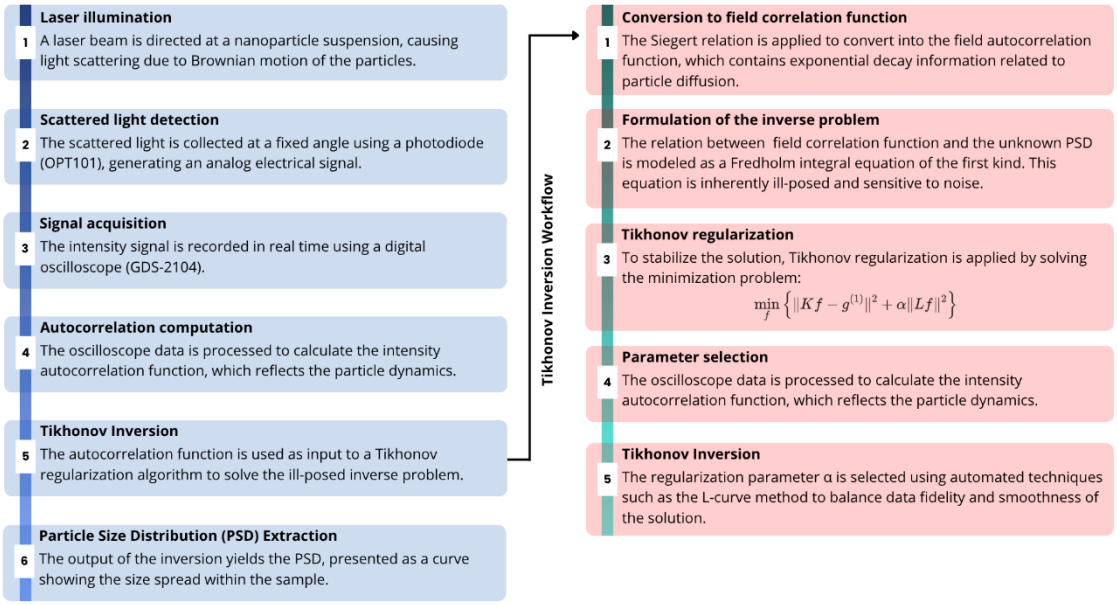

Figure 2. Overview of the experimental and inversion workflow for oscilloscope-based DLS. The left panel shows the measurement steps, including laser illumination, scattered light detection, oscilloscope signal acquisition, and autocorrelation computation. The right panel illustrates the numerical inversion procedure, where the intensity autocorrelation function is converted to the field correlation function, formulated as a Fredholm integral equation, and solved using Tikhonov regularization with parameter selection via the L-curve method. The final output is the PSD.

Once the intensity signal is acquired, the data are processed to compute the intensity autocorrelation function, which quantifies how quickly the speckle pattern produced by the scattered light loses memory of its initial state. This autocorrelation function is central to DLS because its decay rate is directly related to the diffusion coefficient of the particles and, consequently, their hydrodynamic diameter. However, the intensity autocorrelation function must first be converted into the field autocorrelation function using the Siegert relation, which establishes the theoretical link between measured intensity fluctuations and the underlying optical field.

The next step formulates the particle sizing problem as an inverse problem. The field autocorrelation function is mathematically expressed as a Fredholm integral equation of the first kind, where the unknown PSD appears inside an integral kernel composed of exponential decay terms. Such integral equations are ill-posed, meaning that small amounts of noise in the measured data can lead to large instabilities in the reconstructed PSD if solved directly. To address this challenge, Tikhonov regularization is employed

to stabilize the inversion. This method seeks a PSD that simultaneously fits the measured data and remains smooth or physically meaningful by minimizing a composite cost function consisting of a data fidelity term and a regularization penalty weighted by a parameter α.

Selecting an appropriate value of α is crucial because it determines the balance between faithfully reproducing the measured correlation function and suppressing noise-driven oscillations in the solution. Automated approaches, such as the L-curve method, are used to identify the optimal α by examining the trade-off between the residual norm and the regularization norm across multiple candidate solutions. Once the optimal parameter is chosen, the Tikhonov inversion yields a stable PSD that captures the size distribution of the particles in the sample. The final output is presented as a particle size distribution curve, illustrating how particle sizes are distributed either as differential frequency or cumulative undersize within the nanoparticle suspension.

2.2 Tikhonov Regularization for Inversion Model

The scattered light signal is processed using the second-order autocorrelation function $G_2(\tau)$, which is defined as the integral of the product between the light intensity at time t and at $t + \tau$ [9, 15, 16].

$$G_2(\tau) = \langle I(t) \cdot I(t+\tau) \rangle \tag{1}$$

τ represents the time interval (lag time) between two observation points. In general, DLS instruments export the normalized version of the $G_2(\tau)$ function [9, 11, 16].

$$g^{(2)}(\tau) = \frac{\langle I(t) \cdot I(t+\tau) \rangle}{\langle I(t) \rangle^2} \tag{2}$$

the normalized second-order autocorrelation function $g^{(2)}(\tau)$ is used as the input data for calculating the nanoparticle size distribution.

Next, the signal is converted into the first-order autocorrelation function $g^{(1)}$ using the Siegert relation [9, 15, 16, 17]:

$$g^{(2)} = 1 + \beta \left| g^{(1)}(\tau) \right|^2 \tag{3}$$

$$g^{(1)} = \pm \sqrt{\frac{g^{(2)} - 1}{\beta}} \tag{4}$$

where β is the coherence factor of the detection system. Equation (4) also indicates that the computation is valid only when the condition $g^{(2)}(\tau) \geq 1$ is satisfied.

The relationship between the first-order autocorrelation function $g^{(1)}(\tau)$ and the standard distribution function of the decay rates $G(\Gamma)$ is modeled using a first kind Fredholm integral equation expressed as follows [18, 19]:

$$g^{(1)}(\tau) = \int_0^\infty K(\tau, s) f(s)\, ds \tag{5}$$

In the context of DLS, the first-kind Fredholm integral in Equation (5) can be expressed as follows [6, 9, 16]:

$$g^{(1)}(\tau) = \int_0^\infty \exp(-\Gamma\tau) G(\Gamma)\, d\Gamma \tag{6}$$

where τ is the lag time and Γ is the decay rate. To determine Γ the diffusion coefficient is required, which is given by [11, 15, 16]:

$$D = s^{-1} q^{-2} \tag{7}$$

$$q = \frac{4\pi\eta_0}{\lambda_0} \sin\left(\frac{\theta}{2}\right) \tag{8}$$

where s is the inverse of the decay constant, q is the scattering (Bragg) wavevector, η_0 is the refractive index of the solvent, λ_0 is the wavelength of the incident laser light, and θ is the scattering angle.

The discrete form of Equation (6) is written as [8, 9]:

$$g^{(1)}(\tau_j) = \sum_{i=1}^{n} \zeta_i \exp\left(-\frac{\tau_j}{s_i}\right) \tag{9}$$

where ζ_i epresents the scattering intensity contribution of particles in size class i, s_i denotes the inverse decay rate of size class i, the index i corresponds to the particle size sequence, and the index j corresponds to the lag-time sequence of the measured autocorrelation data.

Equation (9) can be represented as a linear relationship as shown in Equation (10) [6, 15,17].

$$\boldsymbol{g} = \boldsymbol{A}\boldsymbol{x}, \qquad \boldsymbol{x} = [\zeta_1, \zeta_2, \ldots, \zeta_n]^T \tag{10}$$

the vector $g^{(1)}(\tau_j)$ is denoted as $\boldsymbol{g}$, while the term $\exp\left(-\frac{\tau_j}{s_i}\right)$ is represented by the matrix $\boldsymbol{A}$ as shown in Equation (11), and $\boldsymbol{x}$ is the set of unknowns with elements ζ_i.

$$\boldsymbol{A} = \begin{bmatrix} \exp\left(-\frac{\tau_1}{s_1}\right) & \exp\left(-\frac{\tau_1}{s_2}\right) & \ldots & \exp\left(-\frac{\tau_1}{s_{200}}\right) \\ \exp\left(-\frac{\tau_2}{s_1}\right) & \exp\left(-\frac{\tau_2}{s_2}\right) & \ldots & \exp\left(-\frac{\tau_2}{s_{200}}\right) \\ \vdots & \vdots & \ddots & \vdots \\ \exp\left(-\frac{\tau_{500}}{s_1}\right) & \exp\left(-\frac{\tau_{500}}{s_2}\right) & \ldots & \exp\left(-\frac{\tau_{500}}{s_{200}}\right) \end{bmatrix} \tag{11}$$

the indices *i* and *j* are obtained directly from the experimental data, where i corresponds to the particle size sequence and *j* corresponds to the number of lag-time points in the autocorrelation function. In this representation, the value 200 corresponds to the number of discrete size classes selected to construct the particle size distribution, meaning that the decay rates s_i are sampled across 200 logarithmically spaced values to span the full diameter range of interest. Meanwhile, the value 500 represents the number of autocorrelation points obtained from the oscilloscope (GDS-2104) during the signal acquisition process, which determines the number of lag-time entries τ_j used in the

construction of the autocorrelation function. Thus, the dimensions of matrix $\boldsymbol{A}$ reflect the experimental configuration, 500 lag-time points in the correlation data and 200 candidate size bins used in the inversion process.

The solution to the linear system in Equation (10) is ill-posed, Tikhonov regularization is employed by minimizing [6, 8, 17, 19]:

$$\min_{x\geq 0} \Upsilon(x) = ||Ax - g||_2^2 + \alpha^2 ||Lx||_2^2 \tag{12}$$

where α is the regularization parameter and L is a finite-difference second-order operator that enforces smoothness (penalizes curvature) on the solution. Consequently, the term $||Lx||_2^2$ is expressed as

$$||Lx||_2^2 = (\zeta_{i+1} - 2\zeta_i + \zeta_{i-1})^2 \tag{13}$$

The operator L in matrix form is written as follows [14]:

$$L = \begin{bmatrix} 1 & -2 & 1 & 0 & 0 & \cdots & 0 & 0 & 0 \\ 0 & 1 & -2 & 1 & 0 & \cdots & 0 & 0 & 0 \\ 0 & 0 & 1 & -2 & 1 & \cdots & 0 & 0 & 0 \\ \vdots & \vdots & \vdots & \ddots & \ddots & \ddots & \vdots & \vdots & \vdots \\ 0 & 0 & 0 & \cdots & 1 & -2 & 1 & 0 & 0 \\ 0 & 0 & 0 & \cdots & 0 & 1 & -2 & 1 & 0 \\ 0 & 0 & 0 & \cdots & 0 & 0 & 1 & -2 & 1 \end{bmatrix}_{198\times 200} \tag{14}$$

To determine the optimal value of α, the L-curve method is employed by plotting $\Lambda(x)$ as the independent variable and $\lambda(x)$ as the dependent variable (see Equation (15)) [15]. The value of $\alpha$is searched within the range of 10^{-6} to 10^{6}, and the optimal α is selected at the point located near the corner of the resulting L-shaped curve.

$$\Lambda(\mathrm{x}) = \log(||Ax - g||_2^2), \qquad \lambda(x) = \log\left(\alpha||Lx||_2^2\right) \tag{15}$$

The optimal value of α is then used to solve the Tikhonov regularization problem in Equation (12), where the resulting solution is the vector ζ_i.

To compute the diffusion coefficient D, the values of ζ_i are substituted into Equation (7). The diffusion coefficient is subsequently used in the Stokes–Einstein equation (Equation (16)) to calculate the hydrodynamic radius R_h [11, 16].

$$R_h = \frac{k_b T}{6\pi\mu D} \tag{16}$$

where k_B is the Boltzmann constant, T is the temperature of the DLS system, and μ is the viscosity of the sample. The calculated value of R_h is then used to determine the PSD for indices $i = 1$ to $i = 200$. To ensure that the PSD data are valid and physically meaningful, normalization is applied to the resulting PSD curve.

3. Result and Discussion

The results obtained from the oscilloscope-based DLS system reveal a clear relationship between the acquisition parameters and the quality of the reconstructed particle size distributions. By analyzing both the L-curve regularization profiles and the resulting PSD curves, it becomes evident that the temporal resolution of the oscilloscope plays a critical

role in determining the stability, sharpness, and accuracy of the inversion output. Variations in time/div settings directly influence the noise level in the autocorrelation function, the optimal regularization parameter α, and ultimately the position and width of the extracted PSD peaks. When these results are compared with those produced by a commercial DLS instrument, the differences and similarities between the two measurement approaches become more pronounced, allowing a comprehensive evaluation of the performance, limitations, and reliability of the self-constructed DLS system.

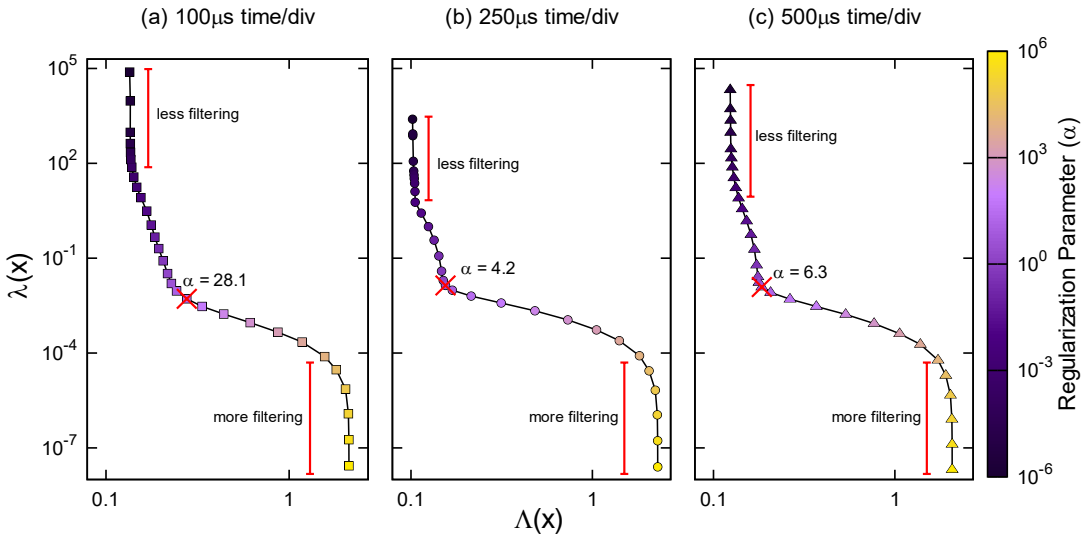

Figure 3. Graph of L-curve method for Tikhonov regularization to get the best regularization value (α) at different time resolution on oscilloscope (a) 100μs time/div; (b) 250μs time/div; (a) 500μs time/div.

Figure 3 shows the L-curve profiles obtained from Tikhonov regularization for three oscilloscope acquisition settings, namely 100 μs, 250 μs, and 500 μs time/div. Each curve illustrates the characteristic balance between the residual norm and the solution norm as the regularization parameter α varies, enabling identification of the optimal α at the corner of the curve. In the left region of the curve, where the residual norm becomes very small and the solution norm increases sharply, the system enters an over-fitting regime characterized by insufficient filtering (less filtering). In this region, α is too small, causing the inversion to fit noise-dominated fluctuations of the autocorrelation data. Conversely, in the upper right region of the curve, where the solution norm becomes overly damped and the residual norm is large, the system falls into an under-fitting regime with excessive filtering (more filtering), indicating that α is too large and the fine structural features of the underlying particle size distribution are suppressed. The optimal operating point, located at the L-curve corner, provides the best compromise between these two extremes and yields a physically meaningful inversion result.

For the shortest sampling window of 100 μs, the L-curve displays a sharp bend with the optimum located near α = 28.1. This higher α value indicates that stronger filtering is required because short acquisition windows typically introduce higher noise into the autocorrelation function, thus demanding more aggressive smoothing to stabilize the inversion. When the time/div is increased to 250 μs, the L-curve becomes smoother and the corner shifts downward to α = 4.2, reflecting an improved signal to noise ratio due to the longer sampling duration. In this case, the autocorrelation signal is less noisy and therefore the inversion can be performed with much weaker regularization, preserving

more information about the underlying particle dynamics. At the longest sampling interval of 500 μs, the optimal α increases slightly to approximately 6.3. Although the noise level is generally reduced at longer acquisition times, excessively long sampling windows may reduce temporal resolution and flatten the autocorrelation decay, thereby requiring a moderate level of regularization to compensate for the loss of structural detail in the signal.

Taken together, these observations reveal that the choice of time/div strongly influences the regularization strength needed for stable inversion: short time/div requires high α due to noise, intermediate time/div yields the smallest α due to optimal balance between noise and resolution, and very long time/div results in a moderate α owing to reduced temporal sensitivity. Overall, the 250 μs condition provides the most efficient compromise, producing the most favorable L-curve shape and the lowest α value, thus offering the best conditions for reconstructing an accurate and stable PSD from the measured autocorrelation data.

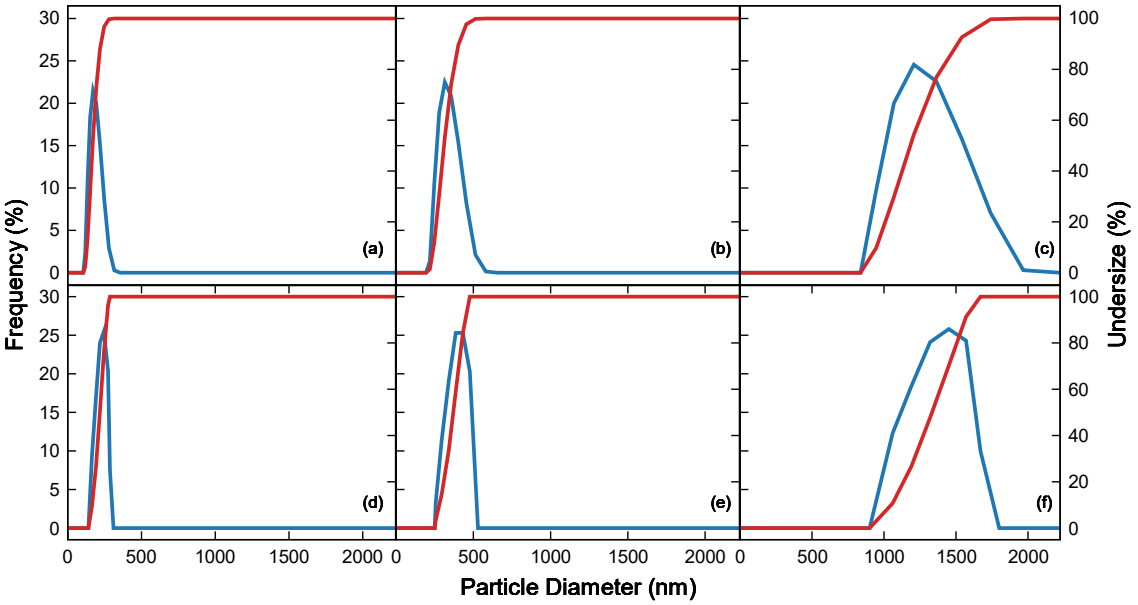

Figure 4. PSD obtained from two different DLS acquisition systems: conventional DLS (panels a–c) and oscilloscope-based DLS (panels d–f). Panels (a), (b), and (c) represent PSD results acquired from a conventional DLS instrument using gate times (GT) of 1.28 μs, 2.56 μs, and 10.24 μs, respectively. Panels (d), (e), and (f) correspond to PSD obtained from the oscilloscope-based DLS system with time/div settings of 100 μs/div, 250 μs/div, and 500 μs/div, respectively. The blue curves indicate the differential particle size distributions (frequency), while the red curves represent the cumulative undersize distributions (% passing).

The PSDs obtained from both the conventional DLS instrument (panels a–c) and the oscilloscope based DLS system (panels d–f) demonstrate a strong degree of consistency across all particle size regimes investigated. For the smallest particle population, shown in panels (a) and (d), the differential PSDs exhibit narrow and sharply defined peaks, while the cumulative undersize curves rise steeply toward 100%, indicating a predominantly monodisperse distribution. The close agreement in peak location and cumulative behavior between the two systems confirms that the oscilloscope-based acquisition with a time/div setting of 100 μs effectively captures the fast intensity fluctuations characteristic of small particle Brownian motion. In the intermediate regime,

represented in panels (b) and (e), both systems reproduce similar peak positions and distribution widths, although minor deviations in peak sharpness can be observed, likely arising from differences in signal to noise ratio and the regularization strength applied during the Tikhonov inversion. Nevertheless, the cumulative curves remain highly congruent, suggesting that key PSD metrics such as D10, D50, and D90 are reliably preserved.

For the largest particle population (panels c and f), where the correlation decay becomes substantially slower, the oscilloscope-based system continues to follow the general trend of the conventional DLS results. While slight broadening and asymmetry in the differential PSD are visible in panel (f), these deviations are expected due to increased sensitivity to baseline drift and longtime noise in low frequency measurements. Importantly, the cumulative undersize curves still converge at similar particle diameters, indicating that the oscilloscope system accurately resolves the global distribution characteristics even for slow-decaying autocorrelation signals. Taken together, these results demonstrate that the oscilloscope-based DLS approach is capable of reproducing PSDs from a commercial DLS instrument with high fidelity across a wide range of particle sizes, provided that the acquisition parameters gate time for the conventional instrument and time/div for the oscilloscope re appropriately matched to the temporal dynamics of the sample. This confirms the feasibility of the proposed low-cost system as a practical alternative for nanoparticle size characterization.

The comparison of PSD obtained from the oscilloscope based DLS system and the commercial DLS instrument is presented in Figure 5.

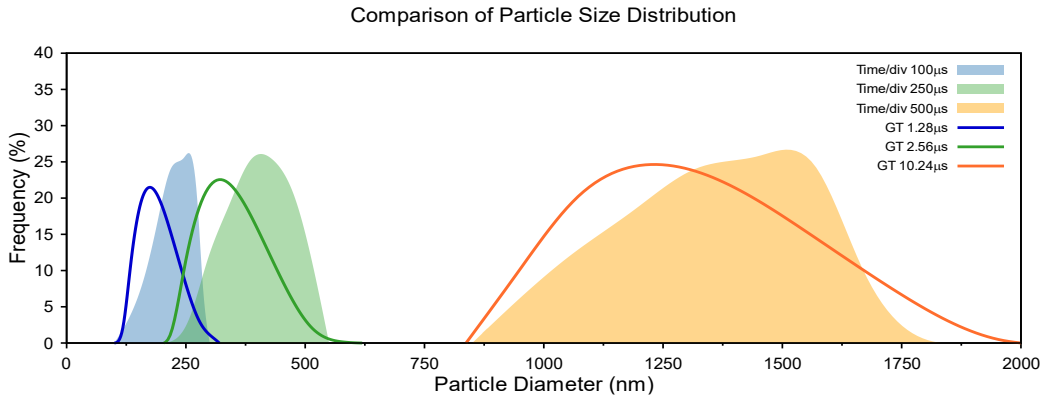

Figure 5. PSD between DLS system based on oscilloscope and commercial DLS system with three variation of time resolution, which the curve comes from commercial DLS system and the shaded comes from oscilloscope DLS system.

The PSD curves from the oscilloscope measurements, represented by the shaded blue, green, and orange distributions corresponding to time/div settings of 100 µs, 250 µs, and 500 µs, exhibit clear unimodal peaks whose positions shift according to the temporal resolution of the acquisition.

The shortest time/div (100 µs) yields a narrow peak centered near ~250 nm, indicating that the higher temporal resolution captures the Brownian decay more precisely, producing a sharper distribution. As the time/div increases to 250 µs and 500 µs, the PSD widens and the mean diameter shifts toward larger values, reflecting the reduced temporal sensitivity and mild oversmoothing observed at longer sampling windows. In contrast,

the PSD curves obtained from the conventional DLS instrument (GT 1.28 μs, 2.56 μs, and 10.24 μs) show similar peak structures but with slightly different peak positions and narrower widths, particularly in the standard measurement range (200–500 nm). The commercial instrument exhibits a sharper and more symmetric peak around ~230 nm (GT 1.28 μs), which serves as a reference for evaluating the accuracy of the oscilloscope based system.

Overall, the oscilloscope derived PSD at 100 μs time/div aligns most closely with the commercial DLS result, both in peak position and overall distribution width, demonstrating that higher sampling resolution improves the fidelity of the inversion process. The 250 μs data also shows reasonable agreement but with slightly broader dispersion, while the 500 μs measurement deviates significantly due to its much wider and shifted peak around the micron scale. This deviation is consistent with the L-curve results, where longer time/div settings required higher regularization and exhibited reduced temporal resolution. These findings confirm that the oscilloscope-based DLS system can reproduce PSD trends comparable to those of a conventional DLS instrument, particularly when operated at optimal time/div conditions, and highlight the importance of precise temporal sampling in achieving accurate particle size reconstruction.

Table 1. Comparison of particle size ranges between conventional DLS (GT) and DIY DLS (Time/div) across different sampling frequencies.

GT (μs)	Size (nm)	Time/div (μs)	Size (nm)
1.28	118 – 315	100	164 – 286
2.56	218 – 580	250	256 – 477
10.24	1068 – 1541	500	1060 – 1670

Table 1 presents a direct comparison of the particle size ranges obtained from the conventional DLS instrument using different gate times (GT) and from the DIY oscilloscope-based DLS system using various time/div settings. The results show a clear correspondence between the two systems across all sampling frequencies. For the smallest particles, the conventional DLS with a GT of 1.28 μs yields a size range of 118–315 nm, while the oscilloscope-based system operating at 100 μs/div produces a slightly broader range of 164–286 nm. Although the lower bound shifts upward in the DIY system, the overall range remains within the same size regime, indicating that the oscilloscope still captures the dominant particle population despite minor differences in temporal resolution. At intermediate sampling frequencies, the conventional DLS operating at a GT of 2.56 μs reports a distribution spanning 218–580 nm, whereas the DIY system at 250 μs/div produces a comparable range of 256–477 nm. Both the lower and upper bounds fall within close agreement, with only modest narrowing observed in the DIY output. This suggests that, at this scale, the oscilloscope maintains adequate sensitivity to resolve the primary distribution while minimizing broadening effects due to noise or limited sampling density.

For the largest particle population, the conventional instrument with a GT of 10.24 μs yields a distribution of 1068–1541 nm. The DIY system, using a 500 μs/div setting, produces a nearly identical range of 1060–1670 nm. This high degree of consistency at large particle sizes demonstrates that the oscilloscope-based setup performs robustly for slowly decaying autocorrelation functions, where long gate times and extended acquisition windows are essential.

Overall, the comparison confirms that the DIY DLS system provides particle size estimates that closely match those of a commercial DLS instrument across small, intermediate, and large particle regimes. Minor deviations in the lower and upper bounds are expected due to differences in temporal resolution, noise characteristics, and acquisition bandwidth between the two measurement approaches. Nevertheless, the general agreement in particle size ranges highlights the viability of the oscilloscope-based method as a reliable and cost-effective alternative for nanoparticle size characterization.

4. Conclutions

Based on the overall results of this study, it can be concluded that the oscilloscope-based self-constructed DLS system is capable of reconstructing particle size distributions with good consistency and demonstrates a significant level of agreement with conventional DLS instruments, particularly when the acquisition parameters are set to their optimal conditions. The L-curve analysis shows that the optimal regularization parameter α is strongly influenced by the temporal resolution, with the 250 μs time/div setting providing the best balance between noise level and signal sensitivity, resulting in the most stable PSD and the closest match to commercial measurements. The comparison of PSD curves further confirms that higher temporal resolution yields sharper and more accurate size distributions without introducing excessive peak shifting. Overall, this work demonstrates that an oscilloscope-based DLS approach can serve as an effective, economical, and flexible alternative for nanoparticle size characterization, while also opening promising opportunities for the development of portable, low-cost DLS systems with competitive accuracy.

References

1. N. Joudeh, D. Linke, Nanoparticle classification, physicochemical properties, characterization, and applications: a comprehensive review for biologists, Journal of nanobiotechnology, Vol. 20 No.1 (2022), p. 1-29.
2. F. Caputo, J. Clogston, L. Calzolai, M. Rösslein, A. Prina-Mello, Measuring Particle Size Distribution of Nanoparticle Enabled Medicinal Products, The Joint View of EUNCL and NCI-NCL. A Step by Step Approach Combining Orthogonal Measurements with Increasing Complexity, Journal of Controlled Release, Vol. 299 (2019), p. 31-43.
3. F. Faizal, S. Saallah, I. W. Lenggoro, Particulate Structures Produced by Electrosprays of Colloidal Silica Suspensions in Both Negative and Positive Zeta Potentials, Advanced Powder Technology, Vol. 29 Issue. 7 (2018), p. 1771-1777.
4. F. Natalia, J. A. Kramar, Dynamic Light Scattering Distributions by Any Means, Journal of Nanoparticle Research, Vol. 23 No. 5 (2021), p. 120.
5. C. M. Maguire, M. Rösslein, P. Wick, A. P. Mello, Characterisation of Particles in Solution – a Perspective on Light Scattering and Comparative Technologies, Science and Technology of Advanced Materials, Vol. 19 No. 1 (2018). P. 732-745.
6. M. Wang, J. Shen, J. C. Thomas, T. Mu, W. Liu, Y. Wang, J. Pan, Q. Wang, K. Liu, Particle Size Measurement Using Dynamic Light Scattering at Ultra-Low Concentration Accounting for Particle Number Fluctuations, Materials, Vol. 14, Issue 19 (2021), p. 5683.

7. A. R. Karow, J. Götzl, P. Garidel, Resolving Power of Dynamic Light Scattering for Protein and Polystyrene Nanoparticles, Pharmaceutical Development and Technology, Vol. 20 No. 1, p. 84-89.
8. C. Li, Z. Dhou, Y. Wang, J. Shen, W. Liu, G. Zhang, Z. Yang, X. Fu, Particle Size Inversion Based on $L_{1,\infty}$-Constrained Regularization Model in Dynamic Light Scattering, Photonics, Vol. 11 No. 11 (2024), p. 1041.
9. O. Burastero, G. D. Barr, B. Raynal, M. Chevreuil, P. England, M. G. Alai, Raynals an Online Tool for The Analysis of Dynamic Light Scattering, Structural Biology, Vol.79, Issue 12 (2023), p. 673-683.
10. Y. Zhang, S. Fu, Q. Z, X. Chen, J. Feng, J. Cui, B. Ai, AI-Enabled Compact and Efficient Dynamic Light Scattering System for Precise Microparticle Sizing, Applied Sciences, Vol. 15 No. 4, p. 1900.
11. J M. Arroyo, J. V. Hernández, J. L. D. Juárez, R. Q. Torres, DLS Home Made Setup: Reviewing First and Second-order Coherence and Autocorrelation Concepts of a Light Source in The Context of Nanoparticle Sizes Synthesized by PLAL, Physica Scripta, Vol. 99 No. 8 (2024), p. 85311.
12. F. Faizal, T. G. Turnip, C. Mulyana, I. M. Joni, C. Panatarani, Dispersion of Geothermal Silica Scaling by Beads Milling Method, AIP Conf, Vol. 2219 No. 1 (2020), p. 080014.
13. A. J. Harvie, S. K. Yadav, J. C. de Mello, A Sensitive and Compact Optical Detector Based on Digital Lock-in Amplification, HardwareX, Vol. 10 (2021).
14. Good Will Instrument Co., Ltd**.**, GDS-2000 Series Oscilloscope Datasheet, GW Instek Documentation, Taiwan (2014).
15. Z. Liu, X. Zhang, Y. Wang, J. Shen, X. Yuan, T. Mu, W. Liu, C. Li, Z. Wang, Research on Tikhonov Regularization Parameter Selection in Dynamic Light Scattering Measurement of Flowing Particles, J ournal of Optics, Vol. 51 No.4 (2022), p. 1038-1051.
16. J. Stefefeld, S. A. McKenna, T. R. Patel, Dynamic Light Scattering: a Practical Guide and Applications in Biomedical Sciences, Biophysical Reviews, Vol. 8 No. 4 (2016), p. 409-427.
17. Y. Wang, Z. Meng, Z. Zhang, M. Xia, L. Xia, W. Li, A Regularization Algorithm of Dynamic Light Scattering for Estimating the Particle Size Distribution of Dual-Substance Mixture in Water, Particuology, Vol. 89, p. 246-257.
18. G. Saparov, Z. Abduvasieva, N. Momunova, T. Matkerimova, V. Tashmatova, Adaptive Regularisation Method for Solving Nonlinear Fredholm Integral Equations of the First Kind, J. of Science and Mathematics Letters, Vol. 13, Issue 2 (2025), p. 17-32.
19. D. Gerth, A New Interpretation of (Tikhonov) Regularization, Inverse Problems, Vol. 37 No. 6 (2021), p. 064002.